Construction and Building Materials 220 (2019) 320–328

Contents lists available at ScienceDirect

Construction and Building Materials

journal homepage: www.elsevier.com/locate/conbuildmat

Synthesis of Fe_3O_4-decorated Mg-Al layered double hydroxides magnetic nanosheets to improve anti-ultraviolet aging and microwave absorption properties used in asphalt materials

Chao Li [a], Shaopeng Wu [a,*], Zongwu Chen [b], Benan Shu [a], Yuanyuan Li [a], Yue Xiao [a], Quantao Liu [a]

[a] State Key Laboratory of Silicate Materials for Architectures, Wuhan University of Technology, Wuhan 430070, China
[b] Faculty of Engineering, China University of Geosciences (Wuhan), Wuhan 430074, China

HIGHLIGHTS

- The M_S value increases from 28.67 emu·g^{-1} to 56.78 emu·g^{-1} with augmented Fe_3O_4-LDHs ratio.
- Fe_3O_4 significantly enhance the anti-UV aging properties and microwave absorption properties of Mg-Al LDHs.
- The maximum R_L value of L_1F_2 is recorded as more than two times of that of LDHs.

ARTICLE INFO

Article history:
Received 11 January 2019
Received in revised form 8 May 2019
Accepted 3 June 2019
Available online 11 June 2019

Keywords:
Mg-Al layered double hydroxides magnetic nanosheets
Fe_3O_4
Anti-ultraviolet aging
Microwave absorption properties
Bitumen modifier

ABSTRACT

Previous studies showed that Mg-Al layered double hydroxides (Mg-Al LDHs) had well anti-ultraviolet (anti-UV) aging properties when used in the asphalt materials, but it cannot contribute to improve the self-healing properties to repair cracks caused by UV aging under the microwave radiation. Fe_3O_4 has well microwave absorption and based on the layered structure and large surface area of Mg-Al LDHs, the primary objective of this work was to synthesize Fe_3O_4-decorated Mg-Al layered double hydroxides magnetic nanosheets, to envisage that the added bitumen modifier has both enhanced anti-UV aging properties and microwave absorption properties. Three modifiers were obtained by the adhesion of Fe_3O_4 magnetic particles on the surface of Mg-Al LDHs nanosheets, and named as L_1F_1 (the mass ratio of LDHs: Fe_3O_4 = 1:1), L_2F_1 (the mass ratio of LDHs: Fe_3O_4 = 2:1) and L_1F_2 (the mass ratio of LDHs: Fe_3O_4 = 1:2). Morphology, phase composition, chemical structure, anti-UV aging properties, static magnetic properties and microwave absorption properties of them were detected by different analytical methods. Results demonstrate that all magnetic nanosheets present the ferromagnetic behavior, L_2F_1 shows the lowest M_S value among three types of magnetic nanosheets, and the value increases from 28.67 emu·g^{-1} to 56.78 emu·g^{-1} with augmented Fe_3O_4-LDHs ratio. Additions of Fe_3O_4 significantly enhance the anti-UV aging properties and microwave absorption properties of Mg-Al LDHs. The maximum R_L value of L_1F_2 is recorded as more than two times of that of LDHs, and L_1F_2 shows the best anti-UV aging properties and microwave absorption properties among all magnetic nanosheets.

1. Introduction

Layered double hydroxides (LDHs) is a type of multifunctional inorganic supramolecular materials, which is formed by the orderly assembly of positively charged metal cation two-dimensional laminate and interlayer anions [1–3]. The nanometer two-dimensional laminates of LDHs are arranged in a longitudinal order to form a three-dimensional crystal structure, which mainly composed of Mg^{2+} and other metal cations [4,5]. The chemical formula of LDHs can be represented by $[M^{2+}_{1-x}M^{3+}_x(OH)_2]^{x+}\cdot(A^{n-})_{x/n}\cdot mH_2O$, where M^{2+} and M^{3+} represent divalent and trivalent metal cations, respectively [6–9].

Studies have shown that the layered structure of LDHs has well shielding effect on ultraviolet rays, and can effectively improve the anti-ultraviolet (anti-UV) aging properties of the asphalt materials [5,10]. Zeng added 3% of Mg-Al layered double hydroxides (Mg-Al LDHs) into AH-90, AH-90 and SBS modified bitumen as anti-UV aging agent. The comparisons of equivalent brittle point and fatigue parameters showed that LDHs could effectively reduce the

* Corresponding author.
E-mail address: wusp@whut.edu.cn (S. Wu).

https://doi.org/10.1016/j.conbuildmat.2019.06.032
0950-0618/

photo-oxidative aging rate of bitumen [11]. This is because when ultraviolet light passes through LDHs, the main layer of metal hydroxide can reflect and absorb ultraviolet light for multiple times. To a certain extent, it can also absorb ultraviolet rays, and the physical shielding effect of the layers on ultraviolet rays is dominant.

In addition, because of the layered structure and large surface area, LDHs can be easily modified with other substances. Li synthesized a sodium stearate modified LDHs (SS-LDHs) and studied the anti-UV aging effects on asphalts mixtures, results showed that the carbonyl index and viscosity aging index of asphalt mixtures contained LDHs or SS-LDHs were lower than those of asphalt mixtures without LDHs and SS-LDHs, proving that LDHs and its modifiers could improve the anti-UV aging performance of asphalt materials [12,13]. Although LDHs can improve the anti-UV aging properties of asphalt materials, it cannot contribute to repair generated cracks and other diseases caused by UV-aging.

However, asphalt materials can be recognized as a type of self-healing materials according to several researches, and generated cracks can be self-closed automatically during the intermittent period of loading [14–17]. The process is due to the elastic recovery, viscous flow and molecular diffusion of bitumen, and can be accelerated at higher temperature heated by microwave radiation or other heating methods.

As shown in Fig. 1, like ultraviolet light, microwave is also a type of electromagnetic waves. The wave length of microwave ranges from 1 mm to 1 m, and its frequency band ranges from 300 MHz to 300 GHz. When microwave penetrates the asphalt materials contained microwave absorbers, it may consume energy through electric loss and magnetic loss. Therefore, microwave absorbers can be mainly classified as two types. For example, carbon fiber [18,19], conductive macromolecule [18] and semiconductor [20] can cause electric loss. Ferrite [21], Fe_3O_4 [22], magnetic metal powder [23] can cause magnetic loss. After absorbing microwave, microwave absorbers can transfer it into other types of energy, Heat release is the main kind of energy transformation under microwave radiation [24,25]. Converted thermal energy can be also called "internal friction heat" and be generated by the high-frequency reciprocating motion of the internal dipole molecules under the microwave radiation. Researchers have applied different microwave absorbers to enhance microwave absorption properties of asphalt materials [26,27]. Li added carbon nanotubes (CNTs) and graphene to improve the heating and healing properties of bitumen under microwave radiation, results indicated that two electric loss microwave absorbers were well in microwave absorption and significantly accelerated the heating process than basis bitumen [15]. Gao explored the feasibility of the usage of steel slag as the aggregate of asphalt mixtures for microwave deicing, and found that steel slag which contained Fe_3O_4 had a well microwave absorption capacity [28].

But these asphalt modifiers have only a single function, they cannot improve the anti-UV aging ability of asphalt materials, and have the ability to enhance the self-healing ability of asphalt materials to repair generated cracks simultaneously. Therefore, in order to envisages that the added bitumen modifier has both enhanced anti-UV aging properties and microwave absorption properties, this paper synthesized different types of magnetic nanosheets, which obtained by the adhesion of Fe_3O_4 magnetic particles on the large surface of Mg-Al LDHs nanosheets with different mass ratio. Firstly, morphology, phase composition and chemical structure of synthesized products were characterized. In addition, anti-UV aging properties, static magnetic properties and microwave absorption properties of them were also detected by different analytical methods.

2. Experimental details

2.1. Materials

All chemicals used in the synthetic procedures were of analytical grade and employed without further purification. Magnesium chloride hexahydrate ($MgCl_2 \cdot 6H_2O$), aluminium chloride hexahydrate ($AlCl_3 \cdot 6H_2O$), ferrous chloride tetrahydrate ($FeCl_2 \cdot 4H_2O$), ferric chloride hexahydrate ($FeCl_3 \cdot 6H_2O$), sodium carbonate anhydrous (Na_2O_3), sodium hydroxide (NaOH) and ammonium hydroxide ($NH_3 \cdot H_2O$) were supplied by Macklin Chemical Reagent Co., Ltd, China.

2.2. Synthesis

As shown in Fig. 2, Fe_3O_4-decorated Mg-Al LDHs magnetic nanosheets were obtained by the following steps: firstly, Mg-Al LDHs was prepared by low saturation coprecipitation method, 2.5 mmol $AlCl_3 \cdot 6H_2O$ and 7.5 mmol $MgCl_2 \cdot 6H_2O$ were dissolved in 100 mL distilled water uniformly, then prepared alkaline solution contained 20 mmol NaOH and 1.25 mmol Na_2O_3 was added simultaneously under vigorous stirring. Secondly, according to in-situ growth method, the Mg-Al LDHs was blended with 5 mmol $FeCl_2 \cdot 4H_2O$ and 2.5 mmol $FeCl_3 \cdot 6H_2O$, and then dispersed in 50 mL methyl alcohol under ultrasonic stirring for 20 min to produce homogenous suspension, $NH_3 \cdot H_2O$ was added dropwise into the suspension till the end of precipitation under ultrasonication. The

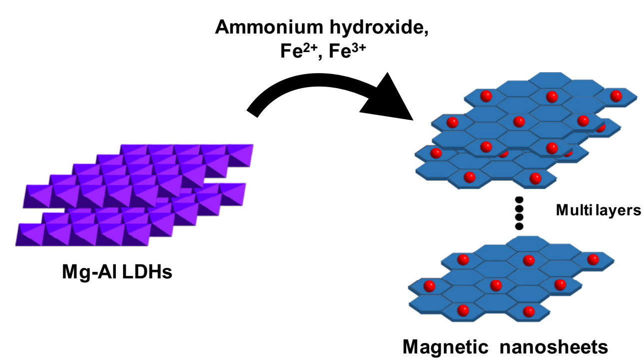

Fig. 2. Schematic diagram of synthesis of Fe_3O_4-decorated Mg-Al LDHs magnetic nanosheets.

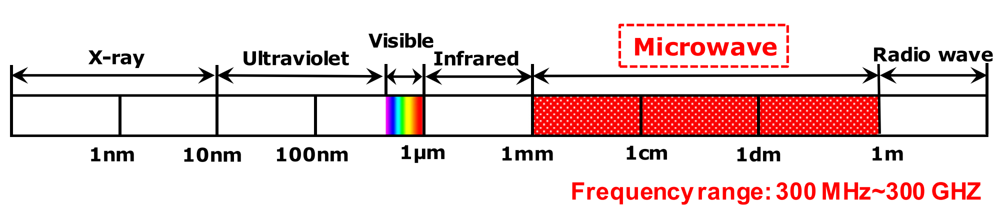

Fig. 1. Graphic introduction of microwave.

resultant (L_1F_1, the mass ratio of LDHs: Fe_3O_4 = 1:1) was separated by a magnet and washed with distilled water and absolute ethanol. The purification was repeated continuously until the effluent solution was neutral, finally the resultant was dried in a vacuum oven at 60 °C for 6 h. For comparison, the Fe_3O_4-decorated Mg-Al LDHs magnetic nanosheets with various Mg-Al LDHs and Fe_3O_4 quantity were synthesized, corresponding to L_2F_1 (the mass ratio of LDHs: Fe_3O_4 = 2:1) and L_1F_2 (the mass ratio of LDHs: Fe_3O_4 = 1:2) at the same conditions.

2.3. Characterization

The morphology, microstructure, phase compositions, chemical structure of as-obtained samples were detected by field-emission Scan Electronic Microscope (FE-SEM, Sigma HD, Zeiss, Germany) with Energy Dispersive Spectrum (EDS), X-ray diffraction (XRD, D8 Advance, Bruker, Germany), Fourier transform infrared spectroscopy (FTIR, Nexus 670, Nicolet, USA).

2.4. Anti-UV aging properties

The anti-UV aging properties of as-obtained samples were detected by Ultraviolet visible spectrophotometer (UV–Vis, Lambda 750S, PerkinElmer, USA). The bandwidth of UV–Vis could be continuously adjusted from 0.17 nm to 5.00 nm, and the wave length ranged from 200 nm to 800 nm. As a result, the change in absorbance (A) with wavelength could be obtained, and greater A value of the substance means better absorption of ultraviolet light.

2.5. Static magnetic properties

The static magnetic parameters were measured by PPMS-9 vibrating sample magnetometer (VSM, Quantum Design, USA), including the residual magnetization (M_r), the saturation magnetization (M_s) and the coercivity (H_c).

2.6. Microwave absorption properties

Based on the coaxial transmission/reflection measurement, electromagnetic parameters of composites were measured through a microwave vector network analyzer system (PNA-N5244A, AGILENT, USA) in the frequency range from 1 GHz to 18 GHz, including the relative complex permittivity ($\varepsilon_r = \varepsilon' - j\varepsilon''$) and relative complex permeability ($\mu_r = \mu' - j\mu''$). The specimens were mixed different magnetic nanosheets with paraffin wax by the weight ratio of 1:1, and pressed to be cylindrical toroidal samples with inner diameter of 3.04 mm, outer diameter of 7.0 mm and height of 2.0 mm. Based on the former analyzed electromagnetic parameters at a given frequency (f) and thickness (t), the reflection loss (R_L) could be used to evaluate the microwave absorption properties of Fe_3O_4-decorated Mg-Al LDHs magnetic nanosheets and calculated using the following equations: $Zn_{in} = Zn_0\sqrt{\mu_r/\varepsilon_r}\tanh\left[j(2\pi fd/c)\sqrt{\mu_r\varepsilon_r}\right]$ and $R_L = 20\log_{10}\left|\frac{Zn_{in}-Zn_0}{Zn_{in}+Zn_0}\right|$. Zn_{in} is the input impedance of material, Zn_0 is the intrinsic impedance at free space, ε_r and μ_r are the relative complex permittivity and permeability of material. R_L value is negative and lower R_L value means stronger attenuate ability of microwave radiation.

3. Results and discussions

3.1. Morphology characterization

Field-emission Scan Electronic Microscope (FE-SEM) was conducted to characterize the morphological difference between Mg-Al LDHs and Fe_3O_4-decorated Mg-Al LDHs magnetic nanosheets. The magnification of 8,000,000 times was adopted in the FE-SEM images.

As shown in Fig. 3, Mg-Al LDHs presents a multilayer structure in nano scale. The nanometer two-dimensional laminates of Mg-Al LDHs are in different size, and arranged in a longitudinal order to form a three-dimensional crystal structure. Original Mg-Al LDHs shows large surface area with smooth appearance. EDS spectra indicates the presence of Mg, Al, O, and C, which are in accordance with the elements of raw materials. After the introduction of Fe_3O_4, Fig. 4 illustrates that the magnetic nanoparticles are randomly decorated on the surfaces of single layer of Mg-Al LDHs and almost form a fusion of Fe_3O_4 and Mg-Al LDHs. The Fe_3O_4 nanoparticles render a cube-like structure and their crystal sizes are all around 200 nm. Moreover, coated Fe_3O_4 nanoparticles make the surface texture of synthesized magnetic nanosheets rougher than that of original Mg-Al LDHs. EDS spectra indicates the presence of Fe, Mg, Al, O, and C, proofing of the presence of decorated Fe_3O_4. As a result, morphology characterizations demonstrate that the Fe_3O_4-decorated Mg-Al LDHs magnetic nanosheets have been synthesized successfully.

3.2. Phase compositions

XRD was applied to evaluate the attachment effect of Fe_3O_4 on Mg-Al LDHs from the perspective of phase composition, and the result was shown in Fig. 5. The diffraction peaks denoted by ♣ appeared at (0 0 3), (0 0 6), (0 1 2), (0 1 5) and (1 1 0) are clearly observed as typical phase of Mg-Al LDHs material. After coating with Fe_3O_4 nanoparticles, the diffraction patterns of L_2F_1, L_1F_1 and L_1F_2 indicate the superimposition of reflections of the Fe_3O_4 and LDHs phase. Among these, the peaks denoted by ♠ appeared at (2 2 0), (3 1 1), (4 0 0), (4 2 2), (5 1 1), and (4 0 0), can be indexed

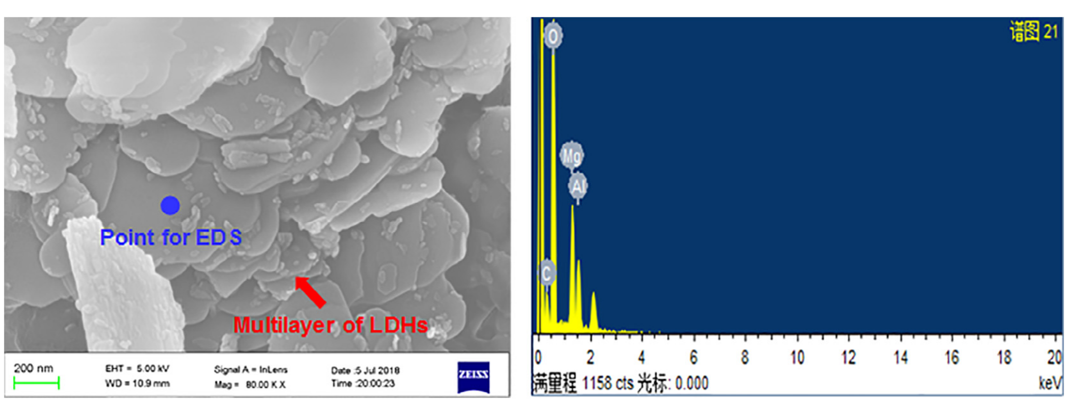

Fig. 3. FE-SEM images and EDS spectra of Mg-Al LDHs.

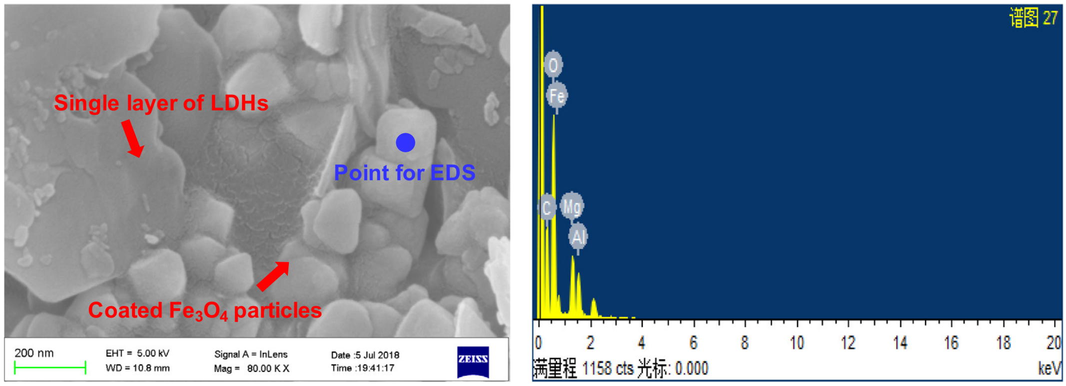

Fig. 4. FE-SEM images and EDS spectra of Fe_3O_4-decorated Mg-Al LDHs magnetic nanosheets.

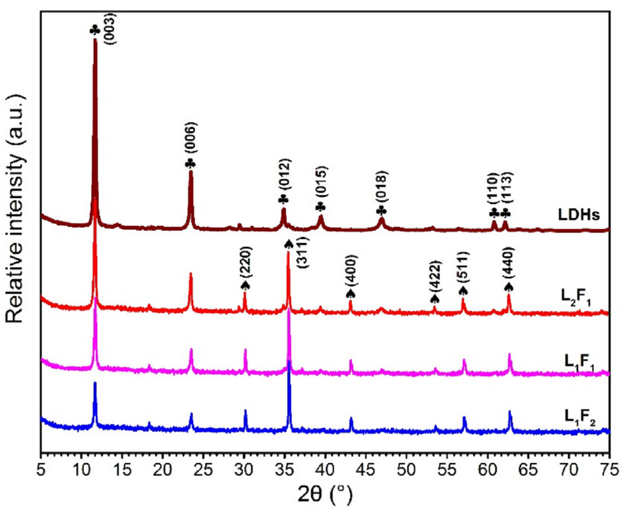

Fig. 5. XRD patterns of Fe_3O_4-decorated Mg-Al LHDS magnetic nanosheets.

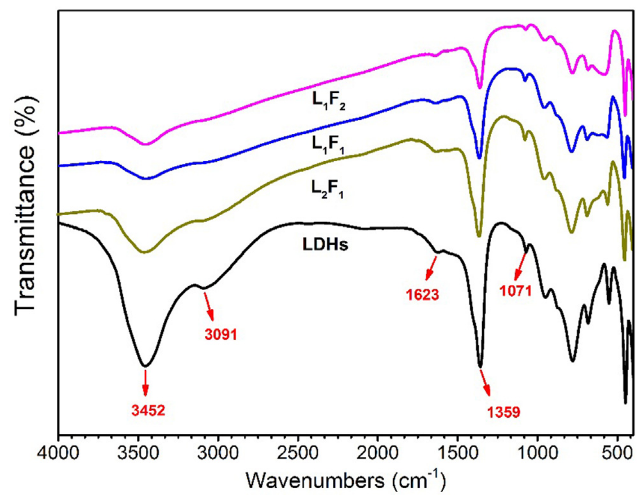

Fig. 6. FTIR spectra of Fe_3O_4-decorated Mg-Al LDHs magnetic nanosheets.

as the characteristic peaks of Fe_3O_4. The characteristic peaks of Mg-Al LDHs at (0 0 3) and (0 0 6) become weaker along with the augment of Fe_3O_4, representing that the Fe_3O_4 occupies larger in the proportion of the synthetic nanosheet. No characteristic peaks of other materials are detected in Fig. 5, representing the high crystallinity of the synthetic magnetic nanosheets.

3.3. Chemical structure

Fig. 6 shows the FTIR spectra of Fe_3O_4-decorated Mg-Al LDHs magnetic nanosheets. In general, 3452 cm^{-1} and 1623 cm^{-1} are attributed to the stretching vibrations of hydroxyl groups and bending vibration of surface-adsorbed water molecules [29,30]. In addition, all samples appear typical peaks of Mg-Al LDHs, adsorption peaks at 3091 cm^{-1} are ascribed to the hydrogen bond between H_2O and CO_3^{2-} in the interlayers of Mg-Al LDHs, the sharp adsorption peak at 1359 cm^{-1} is caused by the stretching vibration of C-O groups [31]. The weak absorption band at 1070 cm^{-1} can be observed and corresponded to stretching vibration of carbonate. the absorption bands in the range of low wave number (400 cm^{-1} - $\sim$ 800 cm^{-1}) are mainly caused by the Al-O, Mg-O, O-Mg-O and O-Al-O in the metal hydroxide sheets in the brucite-like lattice [12]. In the spectra of three magnetic nanosheets, the Fe–O lattice vibration mode of Fe_3O_4 appears at 567 cm^{-1}. Owing to the increasing content of Fe_3O_4, the characteristic peaks of Mg-Al LDHs in as-obtained nanosheets are weakened gradually, while the Fe–O adsorption peak is strengthened and even coincides with the absorption peak next to it in L_1F_2.

3.4. Anti-UV aging properties

Since various substances have different molecules, atoms and different molecular spatial structures, their absorption of ultraviolet light energy will not be the same. Each substance has its own unique and fixed absorption spectrum curve, which can reflect the degree of absorption. Therefore, in this paper, by comparing the degree of absorbance at certain wavelengths in the spectrum, UV–Vis can be used to determine the anti-UV aging properties of different magnetic nanosheets. When the ultraviolet rays pass through the atmosphere to the surface of the asphalt material, greater A value of the substance means better absorption of ultraviolet light. As a result, less ultraviolet light can be absorbed by the asphalt binder, meaning that substance with higher A value processes better anti-UV aging ability when used in the asphalt material.

Fig. 7 presents the UV–Vis results of Fe_3O_4-decorated Mg-Al LDHs magnetic nanosheets, the tested wavelength band includes the UV light (200 nm$\sim$400 nm) and the visible light (400 nm$\sim$800 nm). In the frequency band of UV light, the absorbance of LDHs shows a fluctuating trend and reaches the maximum of 0.2 A at a wavelength of 258 nm. The curve then gradually decreases and the absorbance of Mg-Al LDHs remains constant at around 0.03 A over the visible light range. Former research found

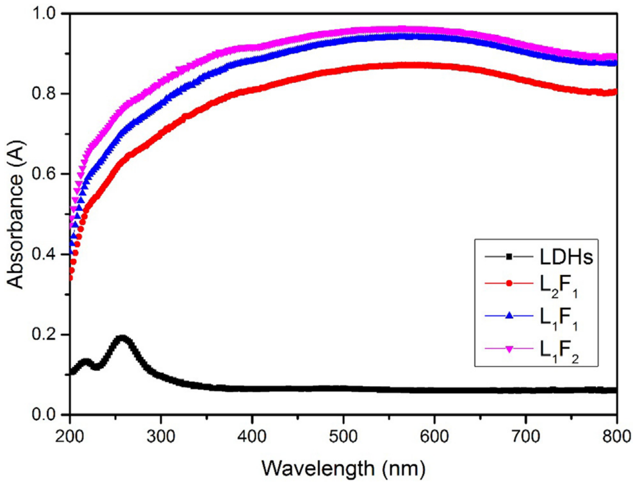

Fig. 7. UV–Vis results of Fe_3O_4-decorated Mg-Al LDHs magnetic nanosheets.

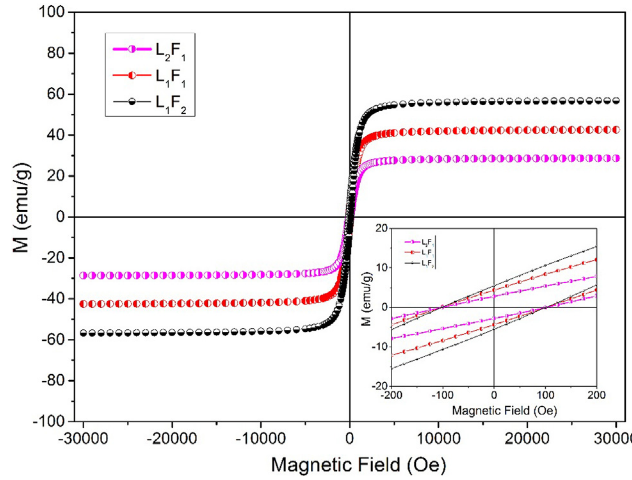

Fig. 8. Magnetic hysteresis loops of all samples, the lower right inset shows the expanded region around the origin.

that the atmosphere has a selective absorption effect on ultraviolet light, short-wavelength ultraviolet rays with high-energy are absorbed by the atmosphere, and the main ultraviolet rays reaching the surface are in the middle and long wavelength bands (280 nm to 400 nm) [12]. Thus, in contrast to former results of Mg-Al LDHs, the absorbance values of Fe_3O_4-decorated Mg-Al LDHs magnetic nanosheets show a rapid increase in the wavelength ranging from 280 nm to 400 nm. In addition, higher ratio of Fe_3O_4 in magnetic nanosheets presents higher absorbance value. Results demonstrate that Fe_3O_4 significantly enhance the anti-UV aging properties of Mg-Al LDHs, and L_1F_2 processed the best anti-UV aging properties among all Fe_3O_4-decorated Mg-Al LDHs magnetic nanosheets.

3.5. Static magnetic properties

Static magnetic properties include the saturation magnetization (M_s), the residual magnetization (M_r) and the coercivity (H_c). The saturation magnetization means if a magnetic substance is placed in a magnetic field whose magnetization increases in magnitude as the magnetic field strength increases, there is a limit on the magnitude of the magnetization. When this limit is reached, the magnitude of the magnetization will no longer increase as the strength of the magnetic field increases, this limit is also called the saturation magnetization. The residual magnetization means after the magnet is placed in a magnetic field, it will generate magnetization, but if the magnetic field is removed, the magnetization will not decrease to zero, and the remaining part is called residual magnetization. The coercivity means in order to make the magnetization become 0, it is necessary to add a magnetic field of a certain magnitude in the opposite direction of the original magnetization direction. This magnetic field is called a coercive magnetic field, also named as the coercivity, and the coercivity can be used to characterize the resistance of the permanent magnet material, and the ability to externally reverse magnetic fields or other demagnetization effects. These three parameters can reflect basic properties of magnetic substance, and suitable M_s and H_c can contribute to obtain well microwave absorption.

It can be seen from the Fig. 8 that the *M-H* hysteresis loops of all samples show a typical S-type curves. In addition, when the applied magnetic field reaches 5000 Oe, almost all samples reach saturation magnetization, indicating the presence of ferromagnetic behavior. If materials have ferromagnetic behavior and is magnetized by the action of an external magnetic field, even if the external magnetic field disappears, the magnetization state of the ferromagnetic materials can be maintained. The ferromagnetic materials have large hysteresis losses, which can improve the microwave absorption. L_2F_1 shows the lowest M_S value among three types of magnetic nanosheets, and the value increases from 28.67 emu·g^{-1} to 56.78 emu·g^{-1} with augmented Fe_3O_4-LDHs ratio shown in Table 1. The M_S value of L_1F_2 is 49.51% higher than that of L_2F_1, this can be expressed by the following facts that according to the relationship $M_s = \Phi m_s$ [32], M_S is related to the volume fraction (Φ) and saturation magnetization (m_s) of individual particle. As Mg-Al LDHs belongs to non-magnetic materials while Fe_3O_4 belongs to magnetic materials, so m_s of individual particle increases with the augment of Fe_3O_4, resulting in a higher M_s of L_1F_2. H_c mainly depends on various types of anisotropy, such as crystal, shape, stress, external inducement and exchange, all as-obtained products show similar and well H_c (>100 Oe).

3.6. Microwave absorption properties

Fig. 9 shows the real part of complex permittivity (ε'), the imaginary part of complex permittivity (ε''), the real part of complex permeability (μ') and the imaginary part of complex permeability (μ'') of the Fe_3O_4-decorated Mg-Al LDHs magnetic nanosheets at the frequency band ranging from 1 GHz to 18 GHz.

As shown in Fig. 9, the L_1F_2 exhibits the highest ε' value while the ε' value of L_2F_1 is the lowest of three as-synthesized samples. In addition, the ε' values of all samples presents a higher value than that of the pure Mg-Al LDHs, and doped Fe_3O_4 made a considerable contribution to the augment of ε' values. The ε'' values indicate a trend of increasing volatility with frequency, and show no evidential difference among all samples. The ε'' values of all samples have shoulder peaks at around 3.5 GHz, 9.5 GHz and 15 GHz frequency positions. In general, the ε' reflects the storage capability of electric energies, depending on space charge and interface polarizations for isotropic crystal cells [33–35]. The increase of ε' value is owing to the enhanced interface polarizations from Fe_3O_4 nanoparticles. The ε'' means the loss ability of stored electric energies, caused by a delay in polarization towards to an altering electrical field in a dielectric medium, and can be classified as intrinsic and extrinsic losses [33]. Crystal structure determines the intrinsic loss which can be described by the interaction of the phonon system with the ac electric field. Imperfections in the crystal structure affects the extrinsic losses, such as impurities, microstructural defects, grain boundaries, porosity, microcracks, and random crystallite orientation [36]. The ε'' values of three as-synthesized samples

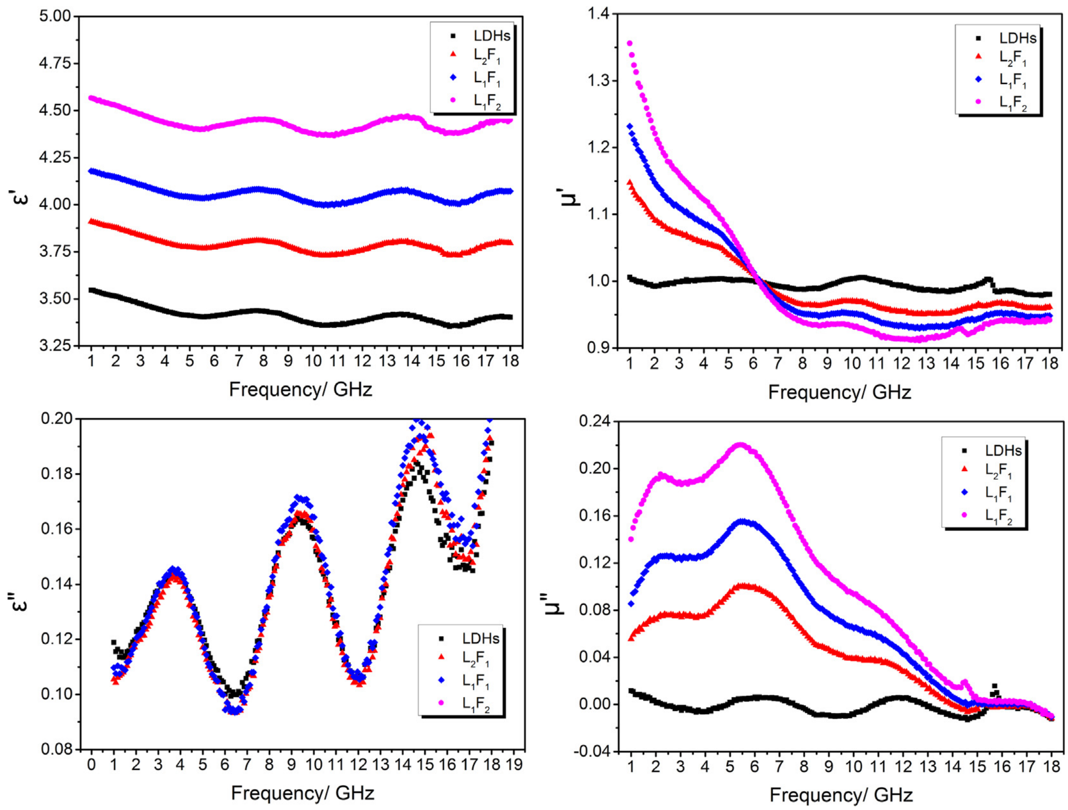

Fig. 9. Electromagnetic parameters of Fe_3O_4-decorated Mg-Al LDHs magnetic nanosheets.

Table 1
Static magnetic parameters of Fe_3O_4-decorated Mg-Al LDHs magnetic nanosheets.

Sample	M_S/emu·g^{-1}	H_C/Oe	M_r/emu·g^{-1}
L_1F_2	56.78	100.22	5.50
L_1F_1	42.56	100.32	4.34
L_2F_1	28.67	100.30	2.79

fluctuate within 0.09–0.2 and the ratio of Mg-Al LDHs and Fe_3O_4 has no effect on them.

Both the frequency and the ratio of Mg-Al LDHs and Fe_3O_4 significantly alter the real part and imaginary part of complex permeability in Fig. 9. As the original LDHs was nonmagnetic substance, so the μ' and μ'' values remain at 1 and 0. In this case, the additions of Fe_3O_4 affect the complex permeability remarkably. As the frequency increases, the μ' values of three as-synthesized samples take on a descensive trend owing to the eddy current loss and ferromagnetic resonance [37]. At the frequency band from 1 GHz to 6.5 GHz, the contents of Fe_3O_4 promote the μ' values and L_1F_2 achieves the highest μ' value. After reaching the same inflection point that all samples own the same μ' values, the change rules of the μ' values are completely opposite to the previous. The μ'' values of all samples fluctuate with the frequency, the peak value of L_1F_2 is two times of L_2F_1 at around 5.5 GHz. High μ'' value means increased loss capability of the magnetic energy, which is related to the high-volume fraction and M_s nonspherical magnetic particles (e.g., flaky iron particles) and acicular iron particles. As synthesized Fe_3O_4 is in cubic shape and L_1F_2 owns the highest M_s, so it can be observed that L_1F_2 processes the best loss ability of magnetic energy.

Fig. 10 shows the dependence of R_L curves on the thickness, in the low-frequency band (1 GHz–10 GHz), Mg-Al LDHs shows low absorption and the R_L values increase with the thickness. After the additions of Fe_3O_4, R_L values of L_2F_1 show a significant increase at the frequency ranging from 1 GHz to 10 GHz, but no evident variation in high frequency band. With the augment of Fe_3O_4 in the synthesized magnetic nanosheets, R_L values present an enhancement in the whole frequency band for both L_1F_1 and L_1F_2. Evidently, L_1F_2 owns the most outstanding microwave absorption properties.

The 3D R_L mapping plots of different magnetic nanosheets as functions of frequency, sample thickness, are shown in Fig. 11. The peak R_L value of Mg-Al LDHs is observed as −4.79 dB at the frequency of 15.71 GHz with a coating thickness of 8 mm, showing a relatively poor microwave absorption property. Three types of Fe_3O_4-decorated LDHs magnetic nanosheets behaves the maximum R_L values at lower frequency. Among them, L_2F_1 behaves the maximum R_L value of −5.25 dB at 11.88 GHz, corresponding to a coating thickness of 10 mm, L_1F_1 behaves the maximum R_L value of −6.88 dB at 11.71 GHz with a coating thickness of 10 mm. The maximum R_L value of L_1F_2 is recorded as more than two times of that of LDHs, and L_1F_2 shows the best microwave absorption properties among all magnetic nanosheets. Results demonstrate that additions of Fe_3O_4 strengthen the microwave absorption of magnetic nanosheets, especially in the low-frequency band.

4. Conclusions

In this paper, in order to ensure that the added bitumen modifier has both enhanced anti-UV aging and microwave absorption properties when applied the microwave heating self-healing technology, different types of magnetic nanosheets were synthesized. As-obtained products were prepared by the adhesion of Fe_3O_4 magnetic particles on the surface of Mg-Al LDHs nanosheets with different mass ratio. Morphology, phase composition, chemical structure, anti-UV aging properties, static magnetic properties

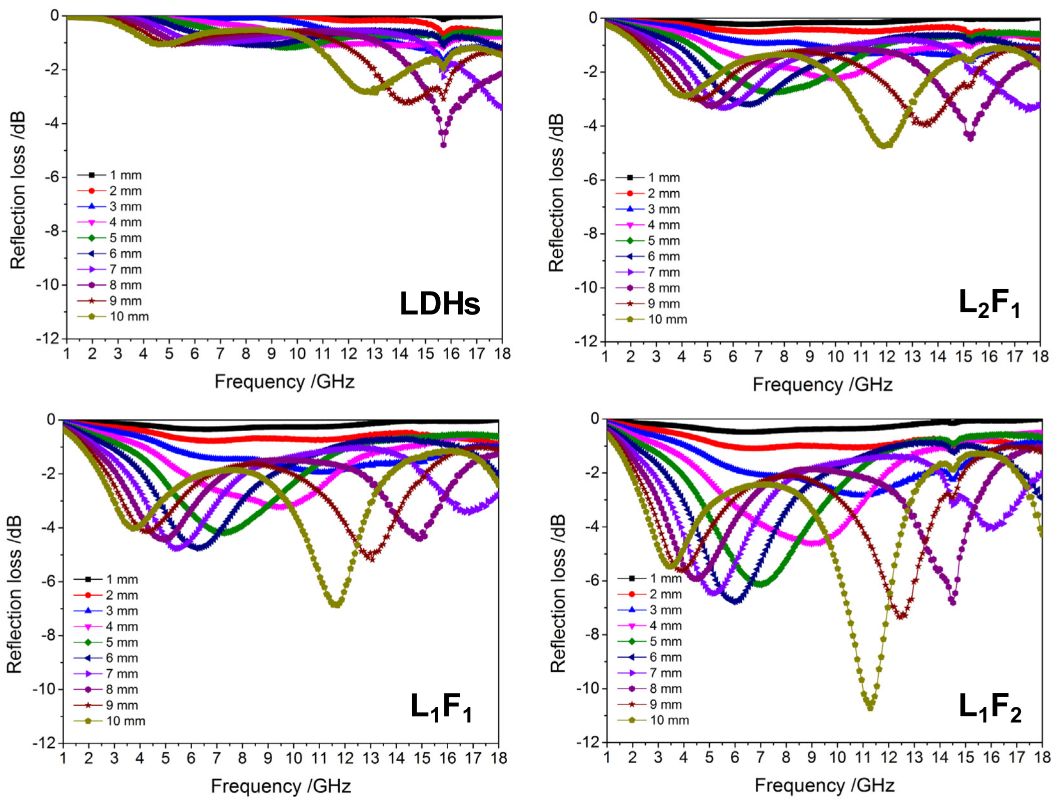

Fig. 10. Reflection loss curves of Fe_3O_4-decorated Mg-Al LDHs magnetic nanosheets.

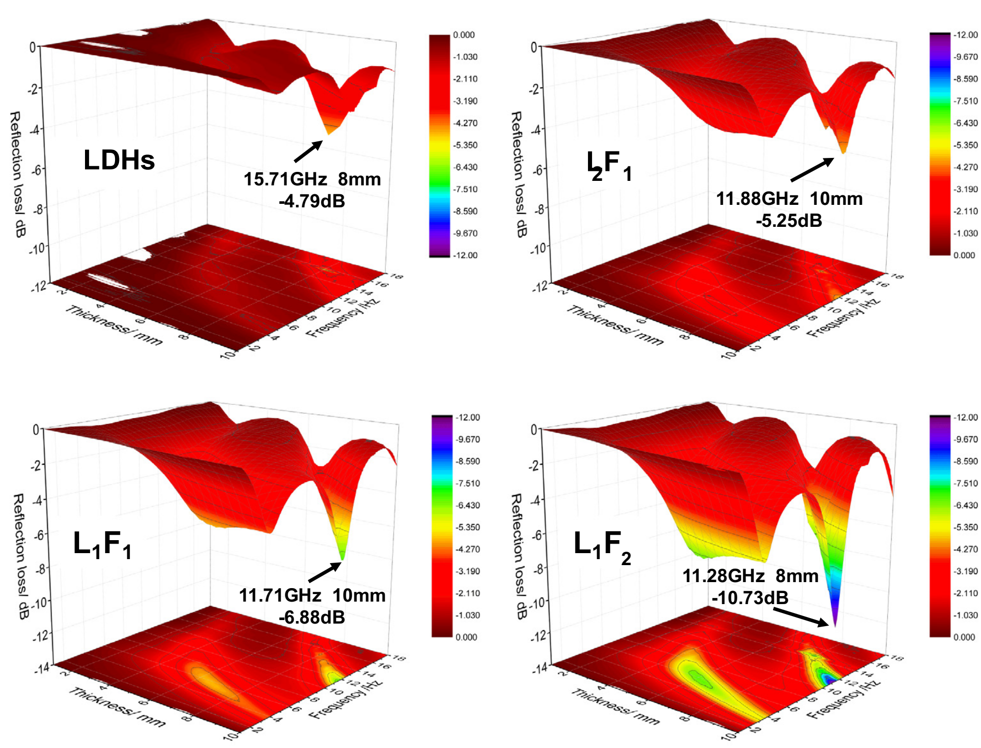

Fig. 11. 3D plots of reflection loss for Fe_3O_4-decorated LDHs magnetic nanosheets.

and microwave absorption properties were detected by different analytical methods. According to the discussed results above, the following conclusions can be obtained:

(1) Because of the layered structure and large surface area, three types of Fe_3O_4-decorated Mg-Al LDHs magnetic nanosheets were successfully synthesized by low saturation coprecipitation method and in-situ growth method according to the characterizations of morphology, phase composition and chemical structure.
(2) The absorbance values of Fe_3O_4-decorated Mg-Al LDHs magnetic nanosheets show a rapid increase in the wavelength ranging from 280 nm to 400 nm, and higher ratio of Fe_3O_4 in magnetic nanosheets presents higher absorbance value. Additions of Fe_3O_4 significantly enhance the anti-UV aging properties of Mg-Al LDHs, and L_1F_2 processed the best anti-UV aging properties among all Fe_3O_4-decorated Mg-Al LDHs magnetic nanosheets.
(3) All magnetic nanosheets indicate the presence of ferromagnetic behavior, L_2F_1 shows the lowest M_S value among three types of magnetic nanosheets, and the value increases from 28.67 emu·g^{-1} to 56.78 emu·g^{-1} with augmented Fe_3O_4-LDHs ratio. In addition, all as-obtained products show similar and well H_c (>100 Oe).
(4) After the additions of Fe_3O_4, R_L values of L_2F_1 show a significant increase at the frequency ranging from 1 GHz to 10 GHz, but no evident variation in high frequency band. With the augment of Fe_3O_4 in the synthesized magnetic nanosheets, R_L values present an enhancement in the whole frequency band for both L_1F_1 and L_1F_2. Evidently, L_1F_2 owns the most outstanding microwave absorption properties.

These results indicate that Fe_3O_4-decorated LDHs magnetic nanosheets can both enhance the anti-UV aging and microwave absorption properties when used in asphalt materials. In practical applications, as long as the raw materials for synthesizing Fe_3O_4 are added to the synthesis process of Mg-Al LDHs, the manufacturers can obtain the Fe_3O_4-decorated LDHs magnetic nanosheets. The raw materials for synthesizing Fe_3O_4 are inexpensive, and do little harm to the HMA production costs in mass output.

Declaration of Competing Interest

There are no conflicts of interest regarding the publication of this paper.

Acknowledgements

This research was funded by National Key R&D Program of China (No. 2018YFB1600200), National Natural Science Foundation of China (71961137010), Fundamental Research Funds for the Central Universities, China (No. 195201013), Natural Science Foundation of China (No. 51778515), Fundamental Research Funds for the Central Universities, China (WUT:182459009) and State Key Laboratory of Silicate Materials for Architectures (Wuhan University of Technology), China, (No. SYSJJ2019-19). Authors also thank the test support from the shiyanjia lab (www.shiyanjia.com), and Wuhan University of Technology for their materials and experimental instruments supports.

References

[1] C.L. Zhang, J.Y. Yu, L.H. Xue, Y.B. Sun, Investigation of gamma-(2,3-Epoxypropoxy)propyltrimethoxy silane surface modified layered double hydroxides improving UV ageing resistance of asphalt, Materials 10 (1) (2017).
[2] P.Q. Cui, H.G. Zhou, C. Li, S.P. Wu, Y. Xiao, Characteristics of using layered double hydroxides to reduce the VOCs from bituminous materials, Constr. Build. Mater. 123 (2016) 69–77.
[3] X.M. Liu, T.Y. Li, H.L. Zhang, Short-term aging resistance investigations of polymers and polyphosphoric acid modified asphalt binders under RTFOT aging process, Constr. Build. Mater. 191 (2018) 787–794.
[4] H.C. Li, J.Y. Yu, S.P. Wu, L. Pang, Y.Y. Li, Y.Q. Wu, Property of anti-ultraviolet aging of LDHs modified asphalt, J. Wuhan Univ. Technol. 33 (3) (2018) 634–638.
[5] C.L. Zhang, J.Y. Yu, S. Xu, L.H. Xue, Z.L. Cao, Influence of UV aging on the rheological properties of bitumen modified with surface organic layered double hydroxides, Constr. Build. Mater. 123 (2016) 574–580.
[6] X. Liu, S.P. Wu, G. Liu, L.P. Li, Effect of ultraviolet aging on rheology and chemistry of LDH-modified bitumen, Materials 8 (8) (2015) 5238–5249.
[7] Y.J. Lin, G.R. Wang, Recent advances in the preparation of layered double hydroxides, Recent Pat. Nanotech. 6 (3) (2012) 169–173.
[8] J.A. Carrasco, G. Abellan, E. Coronado, Influence of morphology in the magnetic properties of layered double hydroxides, J. Mater. Chem. C 6 (5) (2018) 1187–1198.
[9] R. Li, Y. Dai, P. Wang, C. Sun, J. Pei, Evaluation of nano-ZnO dispersed state in bitumen with digital imaging processing techniques, J. Test. Eval. 46 (3) (2017) 20160401.
[10] S. Xu, J.Y. Yu, C.B. Hu, L.J. Jia, L.H. Xue, Evaluation of aging performance of bitumen containing layered double hydroxides intercalated by UV absorbents, Int. J. Pavement Eng. 20 (4) (2019) 499–505.
[11] W.B. Zeng, S.P. Wu, Y. Xiao, Z.W. Chen, Y.H. Sun, Low temperature properties of UV aged asphalts containing layered double hydroxides modifier, J. Appl. Biomater. Func. 14 (2016) S73–S76.
[12] Y.Y. Li, S.P. Wu, Y. Dai, L. Pang, Q.T. Liu, J. Xie, et al., Investigation of sodium stearate organically modified LDHs effect on the anti aging properties of asphalt binder, Constr. Build. Mater. 172 (2018) 509–518.
[13] Y.Y. Li, S.P. Wu, Y. Dai, L. Pang, Q.T. Liu, S. Nie, et al., Laboratory and field evaluation of sodium stearate organically modified LDHs effect on the anti aging performance of asphalt mixtures, Constr. Build. Mater. 189 (2018) 366–374.
[14] A. Garcia, Self-healing of open cracks in asphalt mastic, Fuel 93 (1) (2012) 264–272.
[15] C. Li, S.P. Wu, Z.W. Chen, G.Y. Tao, Y. Xiao, Improved microwave heating and healing properties of bitumen by using nanometer microwave-absorbers, Constr. Build. Mater. 189 (2018) 757–767.
[16] B. Shu, L. Zhang, S. Wu, L. Dong, Q. Liu, Q. Wang, Synthesis and characterization of compartmented Ca-alginate/silica self-healing fibers containing bituminous rejuvenator, Constr. Build. Mater. 190 (2018) 623–631.
[17] X.M. Liu, F.J. Cao, F.P. Xiao, S. Amirkhanian, BBR and DSR testing of aging properties of polymer and polyphosphoric acid-modified asphalt binders, J. Mater. Civ. Eng. 30 (10) (2018).
[18] Z.G. Wang, Q.L. Dai, D. Porter, Z.P. You, Investigation of microwave healing performance of electrically conductive carbon fiber modified asphalt mixture beams, Constr. Build. Mater. 126 (2016) 1012–1019.
[19] R. Li, Q.Q. Guo, Z.L. Shi, J.Z. Pei, Effects of conductive carbon black on PZT/PVDF composites, Ferroelectrics 526 (1) (2018) 176–186.
[20] H. Gao, F. Luo, Q.L. Wen, H.Y. Jia, W.C. Zhou, D.M. Zhu, Enhanced high-temperature dielectric and microwave absorption properties of SiC fiber-reinforced oxide matrix composites, J. Appl. Polym. Sci. 136 (8) (2019).
[21] X.Y. Zhu, Y.S. Cai, S. Zhong, J. Zhu, H.D. Zhao, Self-healing efficiency of ferrite-filled asphalt mixture after microwave irradiation, Constr. Build. Mater. 141 (2017) 12–22.
[22] P.H. Miao, W. Liu, S.Y. Wang, Improving microwave absorption efficiency of asphalt mixture by enriching Fe3O4 on the surface of steel slag particles, Mater. Struct. 50 (2) (2017).
[23] M.A. Franesqui, J. Yepes, C. Garcia-Gonzalez, Top-down cracking self-healing of asphalt pavements with steel filler from industrial waste applying microwaves, Constr. Build. Mater. 149 (2017) 612–620.
[24] Z. Yan, J.H. Luo, Effects of Ce-Zn co-substitution on structure, magnetic and microwave absorption properties of nickel ferrite nanoparticles, J. Alloy. Compd. 695 (2017) 1185–1195.
[25] P.J. Liu, V.M.H. Ng, Z.J. Yao, J.T. Zhou, Y.M. Lei, Z.H. Yang, et al., Microwave absorption properties of double-layer absorbers based on Co0.2Ni0.4Zn0.4Fe2O4 ferrite and reduced graphene oxide composites, J. Alloy. Compd. 701 (2017) 841–849.
[26] A. González, J. Norambuena-Contreras, L. Storey, E. Schlangen, Self-healing properties of recycled asphalt mixtures containing metal waste: An approach through microwave radiation heating, J. Environ. Manage. 214 (2018) 242–251.
[27] J. Norambuena-Contreras, A. Garcia, Self-healing of asphalt mixture by microwave and induction heating, Mater. Des. 106 (2016) 404–414.
[28] G. Jie, A. Sha, Z. Wang, T. Zheng, Z. Liu, Utilization of steel slag as aggregate in asphalt mixtures for microwave deicing, J. Cleaner Prod. 152 (2017) 429–442.
[29] D.K. Cho, S.S. Lee, J.S. Lim, S.H. Baek, I.K. Park, Visible light-emission from Eu-doped ZnAl layered-double hydroxide, Ceram. Int. 43 (13) (2017). S0272884217307484.
[30] C. Gao, X.Y. Yu, T. Luo, Y. Jia, B. Sun, J.H. Liu, et al., Millimeter-sized Mg–Al-LDH nanoflake impregnated magnetic alginate beads (LDH-n-MABs): a novel bio-based sorbent for the removal of fluoride in water, J. Mater. Chem. A 2 (7) (2014) 2119–2128.

[31] D. Yang, X. Wang, W. Ning, G. Zhao, S. Gang, D. Chen, et al., In-situ growth of hierarchical layered double hydroxide on polydopamine-encapsulated hollow Fe3O4 microspheres for efficient removal and recovery of U(VI), J. Cleaner Prod. 172 (2018) 2033–2044.
[32] M.B. Mohamed, K. El-Sayed, Structural, magnetic and dielectric properties of (PANI)–Ni0.5Zn0.5Fe1.5Cr0.5O4 nanocomposite, Compos. Part B Eng. 56 (56) (2014) 270–278.
[33] Y. Liu, T.T. Cui, Y.N. Li, Y.T. Zhao, Y.C. Ye, W.H. Wu, et al., Effects of crystal size and sphere diameter on static magnetic and electromagnetic properties of monodisperse Fe3O4 microspheres, Mater. Chem. Phys. 173 (2016) 152–160.
[34] G.X. Tong, W.H. Wu, Q.A. Hua, Y.Q. Miao, J.G. Guan, H.S. Qian, Enhanced electromagnetic characteristics of carbon nanotubes/carbonyl iron powders complex absorbers in 2–18 GHz ranges, J. Alloy. Compd. 509 (2) (2011) 451–456.
[35] G. Tong, W. Wu, J. Guan, H. Qian, J. Yuan, W. Li, Synthesis and characterization of nanosized urchin-like α-Fe_2O_3 and Fe_3O_4: microwave electromagnetic and absorbing properties, J. Alloy. Compd. 509 (11) (2011) 4320–4326.
[36] S.J. Penn, N.M. Alford, A. Templeton, X. Wang, M. Xu, M. Reece, et al., Effect of porosity and grain size on the microwave dielectric properties of sintered alumina, J. Am. Ceram. Soc. 80 (7) (2010) 1885–1888.
[37] M. Wu, H. He, Z. Zhao, X. Yao, Electromagnetic and microwave absorbing properties of iron fibre-epoxy resin composites, J. Phys. D Appl. Phys. 33 (19) (2000) 2398.